ISSN 0031-918X, Physics of Metals and Metallography, 2017, Vol. 118, No. 11, pp. 1136–1146. © Pleiades Publishing, Ltd., 2017.
Original Russian Text © F.V. Kiryukhantsev-Korneev, A.V. Novikov, T.B. Sagalova, M.I. Petrzhik, E.A. Levashov, D.V. Shtansky, 2017, published in Fizika Metallov i Metallovedenie, 2017, Vol. 118, No. 11, pp. 1202–1213.

STRENGTH AND PLASTICITY

A Comparative Study of Microstructure, Oxidation Resistance, Mechanical, and Tribological Properties of Coatings in Mo–B–(N), Cr–B–(N) and Ti–B–(N) Systems

F. V. Kiryukhantsev-Korneev*, A. V. Novikov, T. B. Sagalova, M. I. Petrzhik, E. A. Levashov, and D. V. Shtansky

National University of Science and Technology MISIS, Moscow, 119049 Russia

**e-mail: kiruhancev-korneev@yandex.ru*

Received March 23, 2017; in final form, May 29, 2017

Abstract—*M*–B–(N) (*M* = Mo, Cr, Ti) coatings were obtained by the magnetron sputtering of MoB, CrB_2, TiB, and TiB_2 targets in argon and in gaseous mixtures of argon with nitrogen. The structure and composition of the coatings have been investigated using scanning electron microscopy, glow-discharge optical emission spectroscopy, and X-ray diffraction. The mechanical and tribological properties of the coatings have been determined by nanoindentation, scratch-testing, and ball-on-disk tribological tests. The experiments on estimating the oxidation resistance of coatings were carried out in a temperature range of 600–1000°C. A distinctive feature of TiB_2 coatings was their high hardness (61 GPa). The Cr–B–(N) coatings had high maximum oxidation resistance (900°C (CrB_2) and 1000°C (Cr–B–N)) and possessed high resistance to the diffusion of elements from the metallic substrate up to a temperature of 1000°C. The Mo–B–N coatings were significantly inferior to the Ti–B–(N) and Cr–B–(N) coatings in their mechanical properties and oxidation resistance, as well as had a tendency to oxidize in air atmosphere after long exposure at room temperature. All of the coatings with nitrogen possessed a low coefficient of friction (in a range of 0.3–0.5) and low relative wear ($(0.8–1.2) \times 10^{-6}$ mm^3 N^{-1} m^{-1}.

Keywords: PVD, coatings, films, magnetron sputtering, titanium, molybdenum, chromium borides, boronitrides, SHS-targets

DOI: 10.1134/S0031918X17110059

INTRODUCTION

The borides of transition metals are promising prospective materials for using as protective coatings for metalworking tools [1], heavily loaded friction units [2], fuel cells [3], parts of aerospace industry [4], etc. due to their high hardness, wear resistance, oxidation and corrosion resistance, diffusion-barrier properties, and low coefficient of friction. The coatings based on Ta–B [5, 6], V–B [7], Ti–B [1, 8, 9], Zr–B [9–11], W–B [12], Ru–B [13], and other alloys were studied for the last two decades. The development of Os–B [14] coatings can be assumed to be promising from the viewpoint of reaching extremely high hardness.

The introduction of nitrogen into the structure of boride coatings makes it possible to form a nanocomposite structure that consists of nanosized crystallites of boride and/or nitride of a transition metal and amorphous interlayers based on boron nitride and showing a unique combination of characteristics, i.e., a hardness above 40 GPa, the elastic recovery of about 70–90%, thermal stability and oxidation resistance up to 900–1000°C [15]. The introduction of nitrogen can have a significant influence on the tribological properties and corrosion resistance of coatings due to the formation of additional amorphous phases and decreasing of crystallite sizes [16]. The earlier works on the boron nitride coatings in the Zr–B–N [17], Hf–B–N [18], V–B–N [19], and Ti–B–N [17] systems should be noted, in which it was shown that controlling the structure, mechanical properties, and wear resistance can be achieved through variations in the nitrogen content in the coatings. Besides the research articles, the active implementation of new grades of boron nitride coatings is carried out by different producers' companies in the market of cutting tools [20].

The investigations of boride and boron nitride coatings described in the literature are usually limited by separate systems, e.g., Hf–B–N [18], V–B–N [19]. In these cases, the information has a scattered character, and it is difficult to compare the coatings between each other because of the different conditions of their deposition. At the same time, this comparison was carried out in some two- and three-component systems, e.g., NbB_2, WB, CrB [21] and Ti–B–N, Zr–B–N, Sc–B–N [9], which made it possible to find the systems that are the most promising for practical

application, as well as to outline the ways to optimize the parameters for depositing coatings. Therefore, comparative studies of coatings obtained in various systems using the same technological regimes are of special interest.

Among the methods used for the deposition of boron nitride coatings, the diffusion saturation, gas-thermal spraying, and chemical and physical vapor deposition are used most frequently. The last method provides universality when selecting the substrates and ensures the high quality of the surface, flexible control of deposition parameters, and, as a consequence, the control of the structure and properties of the material deposited. An analysis of the literature data shows that, among the physical vapor deposition methods, the magnetron sputtering is given special attention (around 50% of articles). The aim of this work is to carry out a comparative study of the structure, mechanical, and tribological properties, as well as the oxidation resistance, of two- and three-component M–B–(N) coatings (M = Mo, Cr, Ti) deposited using the same regimes of the magnetron sputtering of composite targets.

EXPERIMENTAL

Targets for sputtering MoB, TiB, TiB_2, and CrB_2 with diameters of 120 mm and thicknesses of 4–9 mm were obtained by the method of self-propagating high-temperature synthesis (SHS) from elemental powders of metals and boron [22–24]. The magnetron sputtering of the targets was carried out under the same conditions in the dc mode using Pinnacle Plus 5 × 5 (Advanced Energy) power supply, equipped with an arc-suppression system, which makes it possible to keep the desired electric parameters in a continuous mode. The current and voltage values were 2 A and 400–500 V. A bias voltage of –250 V was applied to the substrate during deposition. The sputtering of the targets was performed in an Ar atmosphere and an Ar + N_2 mixture (volume fraction of nitrogen was C_{N2} = 15%) at a pressure of the operating gas of 0.1–0.2 Pa. As the substrates for the deposition of coatings, disks made of the VK6M hard alloy, KhN65VMTYu nickel alloy (deposition time in these cases was 40 min), and plates of KEF-4.5 single-crystal silicon (deposition time was 15 min) were used. The substrates were cleaned in a vacuum by heating to 300°C and subsequent etching with Ar^+ ions with an energy of 1.5–2 keV for 10 min using an ionic source of the slot type. The temperature of the substrate during the deposition was kept at a level of 300–350°C. To determine the oxidation resistance of the coatings and their ability to be a barrier for diffusion of elements from the substrate into the coating upon heating, stepped annealings were carried out at the temperatures 600–1000°C with a step of 100°C and a time of an isothermal holding of 1 h. After each holding and cooling of the sample to room temperature, the depth profile of the distribution of elements was determined. The annealings were performed in air in an SNOL-7.2/1200 muffle furnace.

A PROFILER-2 (Horiba Jobin Yvon) setup was used to record the profile of the contents of the elements and analyze the chemical composition by the glow-discharge optical emission spectroscopy (GDOES) [25]. The transverse fractures of coatings were investigated by the scanning electrons microscopy (SEM) using a Hitachi S4800 microscope in the regime of detection of secondary electron at an accelerating voltage of 20–30 kV. The X-ray diffraction (XRD) analysis was performed in the Bragg–Brentano configuration, as well as using the scheme of a gliding beam with a slope of 5° on a Bruker D8 diffractometer with monochromatized Cu $K\alpha$ radiation. The phase composition of the coatings was additionally analyzed by the method of Raman spectroscopy using a LabRAM HR 800 (Horiba Jobin Yvon) device with a 514-nm-wavelength laser, as well as by the method of infrared spectroscopy using a Vertex-70V device in the reflection mode with an incidence angle of the initiating radiation of 30° relative to the normal to the surface. To determine the mechanical properties of coatings, a Nano-Hardness Tester (CSM Instruments) was used. The depth of the penetration of the indenter under a load of 4 mN did not exceed 10% of the thickness of the coatings. The tribological tests of the coatings were performed using a Tribometer (CSM Instruments) automated friction meter, using the pin-on-disk scheme with a counterbody in the form of a 3-mm ball made of the WC–6% Co alloy at a normal load of 5 N. The wear grooves were investigated using a Wyko-1100NT (Veeco) optical profilometer. The adhesive strength was determined using a Revetest (CSM Instruments) device with the scratching of the surface of the coatings by a Rockwell-C-type indenter with a gradually increasing load. The methods of estimating the mechanical and tribological properties were described in more detail in [16].

RESULTS AND DISCUSSION

According to GDOES, all the elements were distributed uniformly over the depth of the coatings. The content of carbon and oxygen impurities was 1 at % and 2–4 at %, respectively. The presence of impurities can be explained by their presence in both the composition of the targets and the gas phase. The average concentrations of the main elements over the thickness of the coatings are presented in Table 1. In the case of sputtering TiB and MoB targets in argon, the content of boron in the coatings was 42–49 at %, and it decreases regularly to 34–43 at % upon the introduction of nitrogen into the operating gas. The coatings obtained by the sputtering of TiB_2 and CrB_2 targets in argon contained 65–68 at % B with a subsequent decrease in its content to 55–57 at % upon reactive sputtering. In the case of the reactive sputter-

Table 1. Compositions of coatings

Coating	Target	C_{N2}, %	Concentration, at %				
			Ti	Mo	Cr	B	N
1	TiB	0	58 ± 3	–	–	42 ± 2	–
2		15	48 ± 2	–	–	34 ± 2	18 ± 3
3	TiB_2	0	35 ± 2	–	–	65 ± 3	–
4		15	29 ± 2	–	–	55 ± 2	16 ± 1
5	MoB	0	–	51 ± 1	–	49 ± 2	–
6		15	–	47 ± 2	–	43 ± 2	10 ± 2
7	CrB_2	0	–	–	32 ± 2	68 ± 2	–
8		15	–	–	31 ± 2	57 ± 3	12 ± 2

ing, the nitrogen content in the coatings changes depending on the material of the cathode and varies in the range of 10–18 at %, which is probably connected with the different affinity of metallic components for nitrogen.

Figure 1 shows the SEM results of the studies of the morphology of coatings. Note that the detailed morphology of the coatings is not usually clearly revealed in the transverse fractures. For example, the analysis of images shown in Figs. 1a–1f indicates that all coatings have a dense equiaxed structure. However, when observing the fracture that occurred at another angle, in the coating 5 there is observed a fine columnar structure with a transverse size of columnar elements of 10–20 nm (Figs. 1e and 1g). The nanocomposite structure that consists of nanocolumns of somewhat larger size (30–50 nm) separated by amorphous interlayers was previously observed in TiCrBN [26] and TiAlSiCN [27] coatings. Note that the structure of the MoB (5) coating is nevertheless denser than the widely used two-component coatings obtained by the method of the physical vapor deposition (PVD) used in industry (see, e.g., [28, 29]) and, as will be shown below, it possess relatively high mechanical properties.

On the surface of the MoBN coatings, the formation of thin oxide layers (Fig. 1f) was observed by the SEM. Visually, the oxide tints were fixed on the surface of MoB(N) coatings after long exposure in air. The analysis of the elemental composition of the surface of samples carried out by GDOES (Fig. 1h) showed that, in air the samples oxidize slowly with the formation of an MoO_x layer at a rate of approximately 50 nm/year. This is probably connected with the strongly nonequilibrium state of the structure of the MoB(N) coatings.

Figure 2 displays XRD patterns of coatings 1–8. According to XRD data, the base of coating 1 was a TiB phase with an orthorhombic lattice, the characteristic reflections of which were presented at the 2Θ positions of 24°, 29°, 35°, 38°, 42°, and 69° (card no. 01-073-2148 in the JCPDS-ICDD database). This is in good agreement with the data of the elemental analysis, according to which the ratio Ti/B is close to unity in coating 1. The average size of crystallites determined by the Selyakov–Scherrer formula for the TiB phase was 1–2 nm. Apart from the line of the TiB phase, there are also peaks at 57° and 59°, which can be attributed to the TiB_2 phase (card no. 01-089-3923) and silicon substrate, respectively. In the XRD pattern of coating 2, lines of the same phase constituents were observed as for coating 1. The crystallite size of the TiB phase was 1.5 nm. The intensity of the TiB_2 line grew when introducing nitrogen in the composition of the gaseous phase.

According to the XRD data, the only structural component in coating 3 is the TiB_2 phase with a hexagonal lattice, which is characterized by a noticeable texture along the (001) direction that coincides with the direction of the coating growth. The average size of crystallites calculated by the full width at half maximum (FWHM) of lines (001), (100), (101), (002), and (110) was 8–13 nm. The introduction of nitrogen led to a decrease in the crystallite size of the h-TiB_2 phase to 2–3 nm and to a change in the preferential orientation to (101).

The XRD patterns of the Mo–B and Mo–B–N coatings did not differ significantly. Two strongly broadened peaks with the maxima at ~40° and ~70° can be related to the (211) and (213) lines of the t-MoB tetragonal phase (card no. 03-065-2753) or t-Mo_2B (card no. 00-025-0561). The average crystallite size was less than 1 nm (0.6–0.8 nm).

The basis of the coating 7 is a hexagonal h-CrB_2 phase with a strong texture along the (001) direction and average crystallite size of ~3 nm. The nitrogen introduction into the composition of the coating suppresses the formation of the preferential orientation and favors a refinement of the structure (crystallite size ~1.5 nm).

Note that the introduction of nitrogen into the composition of Ti–B, Mo–B, and Cr–B coatings on

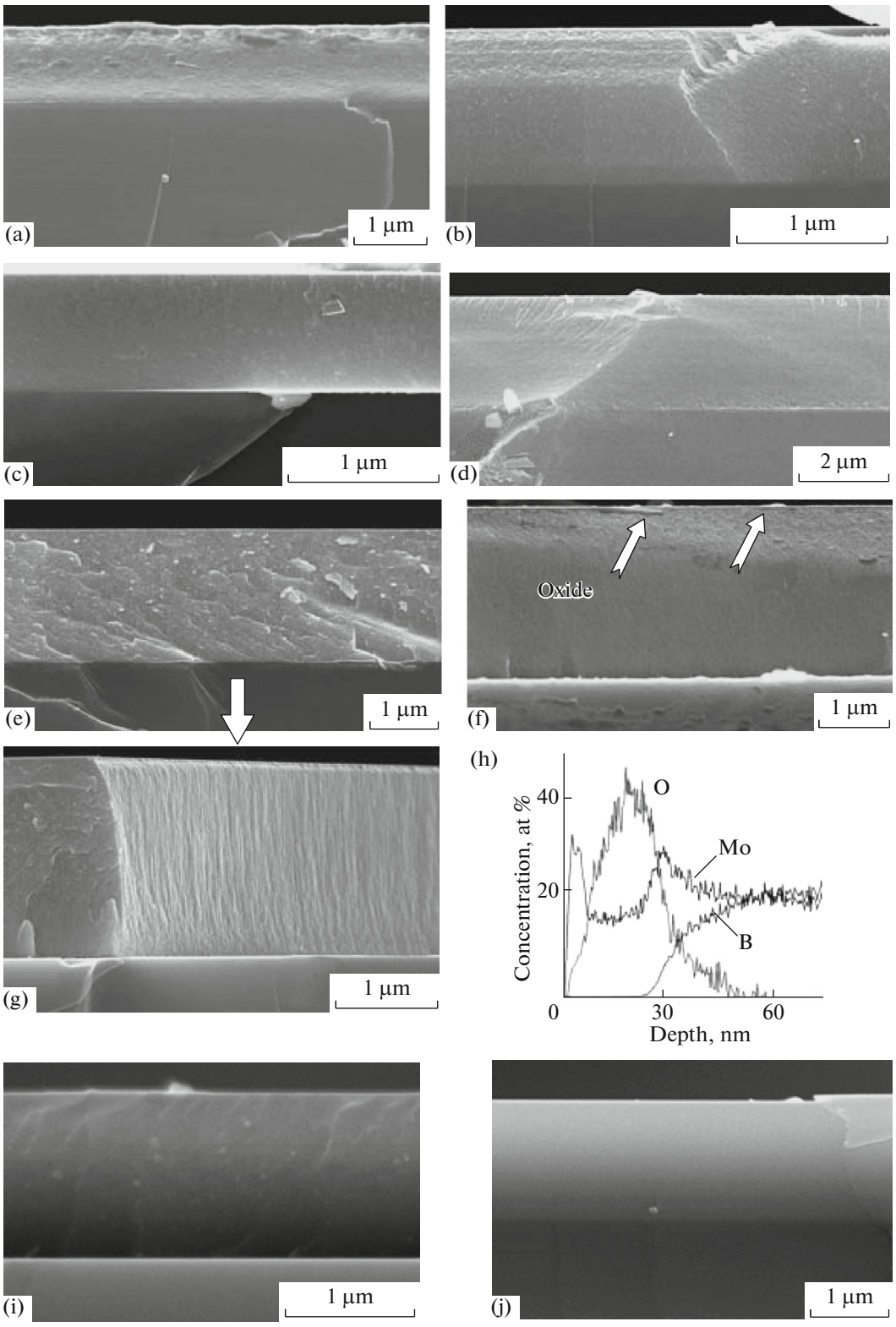

Fig. 1. SEM images of the fractures of coatings (a) 1, (b) 2, (c) 3, (d) 4, (e, g) 5, (f) 6, (i) 7, (j) 8, and (h) GDOES data for the surface of coating 6 after exposure to air for 1 year.

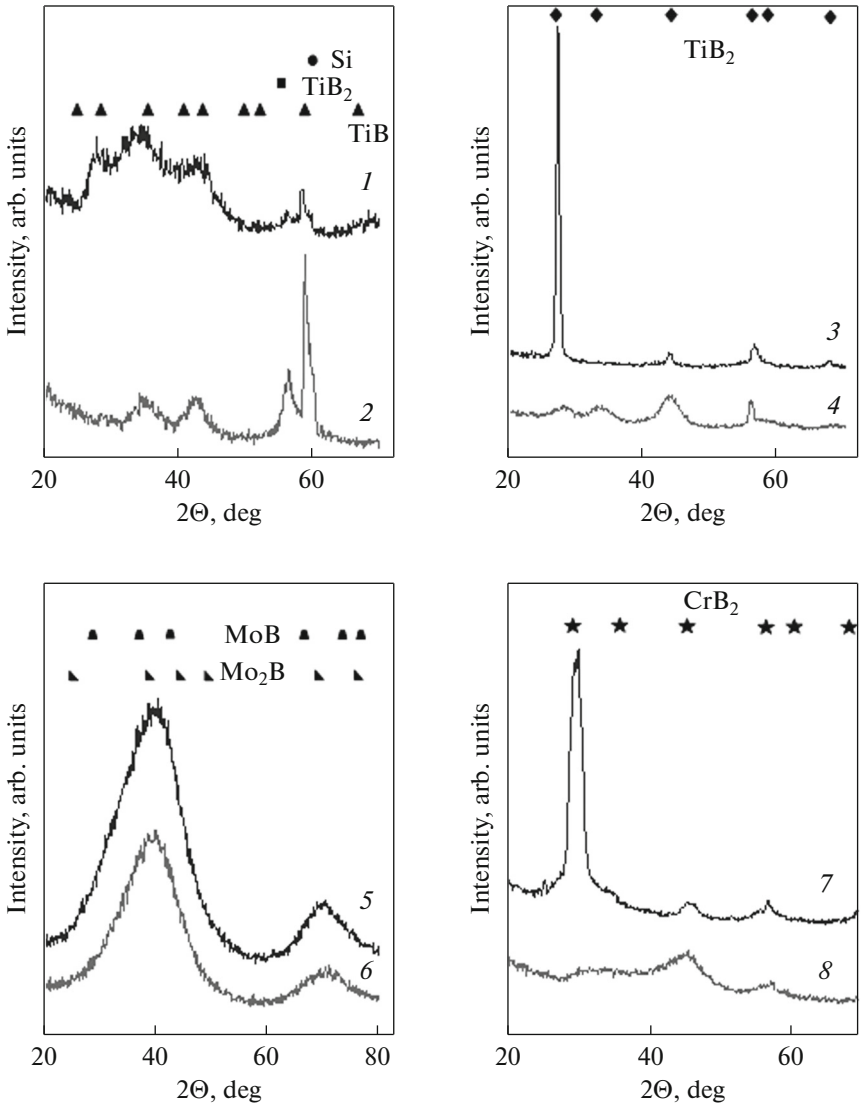

Fig. 2. X-ray diffraction patterns of coatings 1–8 (see Table 1).

the level of 10–18 at % did not lead to the formation of nitrogen-containing crystalline phases. Since no BN phase was observed upon studying the coatings by Raman spectroscopy and infrared spectroscopy (IR), it can be concluded that nitrogen is dissolved in the existing crystalline boride phases. Spectroscopic methods also made it possible to find the presence of bonds with oxygen on the surface, i.e., B–O, B–O–C (880–900 and 1030 cm^{-1} in the IR spectra, respectively) [30, 31], Ti–O (470 cm^{-1} in the IR-spectra) [32], Mo–O (800–880 cm^{-1} in the Raman spectra) [33, 34], and there were no differences observed between the coatings with and without nitrogen. The presence of boron oxide on the surfaces of coatings 1 and 2 was confirmed by XRD upon the measurement using the Bragg–Brentano geometry; a wide peak with a maximum at $2\Theta = 14.6°$ was observed in the XRD patterns, which corresponds to B_2O_3 (card no. 00-013-0570) phase. The presence of traces of H_3BO_3 phase on the surfaces of the coatings also cannot be excluded (wavenumber $\lambda = 880$ cm^{-1} for the Raman spectrum [35] and $2\theta = 14.6°$ for the XRD patterns [36]).

The results of determining the mechanical properties of the coatings deposited on the substrates of VK6M hard alloy are presented in Table 2. For most of the coatings, a decrease in the hardness (H), Young's modulus (E), and elastic recovery (W) was observed upon the introduction of nitrogen. This effect can be related to different factors, such as the decrease in the magnitude of internal compressive stresses, or a change in the texture and decrease in the size of crystallites (the inverse Hall–Petch law). Record values of hardness (on the level of 61 GPa) were obtained for coating 3. To check the values obtained, the Ti–B

Table 2. Mechanical and tribological properties of coatings

Coating	Target	C_{N2}, %	H, GPa	E, GPa	W, %	L_c, N	Vw, $\times 10^{-6}$ $mm^3\,N^{-1}\,m^{-1}$
1	TiB	0	23	270	53	19	16.1
2		15	43	390	72	34	1.1
3	TiB_2	0	61	420	64	27	0.9
4		15	23	250	58	32	1.0
5	MoB	0	27	330	50	>60	21.1
6		15	22	290	48	>60	0.8
7	CrB_2	0	39	380	61	43	18.9
8		15	14	150	54	70	1.2

coatings were deposited by the same regime (beside the VK6M hard alloy) on substrates of the VK-1-0 titanium alloy and the HSS high-speed steel. Repeated measurements were performed using nanohardness meter with a load varies in a range of 4–20 mN. The results of these measurements are shown in Fig. 3. It can be seen that the coating 3 possesses a hardness close to 60 GPa, i.e., it is related to the class of superhard materials. The coincidence of the results of measurements for different types of substrates and different values of loads indicates that the material of the substrate, the penetration depth of the indenter, and the roughness of the coating did not have a significant influence on the results of measurements. The high level of the hardness may be linked to the composition being close to stoichiometric and a high level of compressive stresses [37]. As was shown by the elemental analysis, the coating 3 has a composition close to titanium diboride (B/Ti ratio was 1.86). To estimate the contribution of compressive stresses, the repeated measurements of mechanical properties of the samples after long storage (10 months) during which the partial or full relaxation of stresses took place were carried out. The results have shown that the hardness decreased from 55–61 to 47–52 GPa (Fig. 3b). Thus, the contribution of compressive stresses into the total value of hardness is about 15%.

Apart from the high hardness, the coatings investigated possessed a high elastic recovery, in most cases exceeding 50%. The maximum value of 72% was reached for coating 2 in the Ti–B–N system. The elastoplastic properties (elastic recovery, plasticity index (H/E), and the resistance to plastic deformation (H^3/E^2)) can have a significant influence on the wear

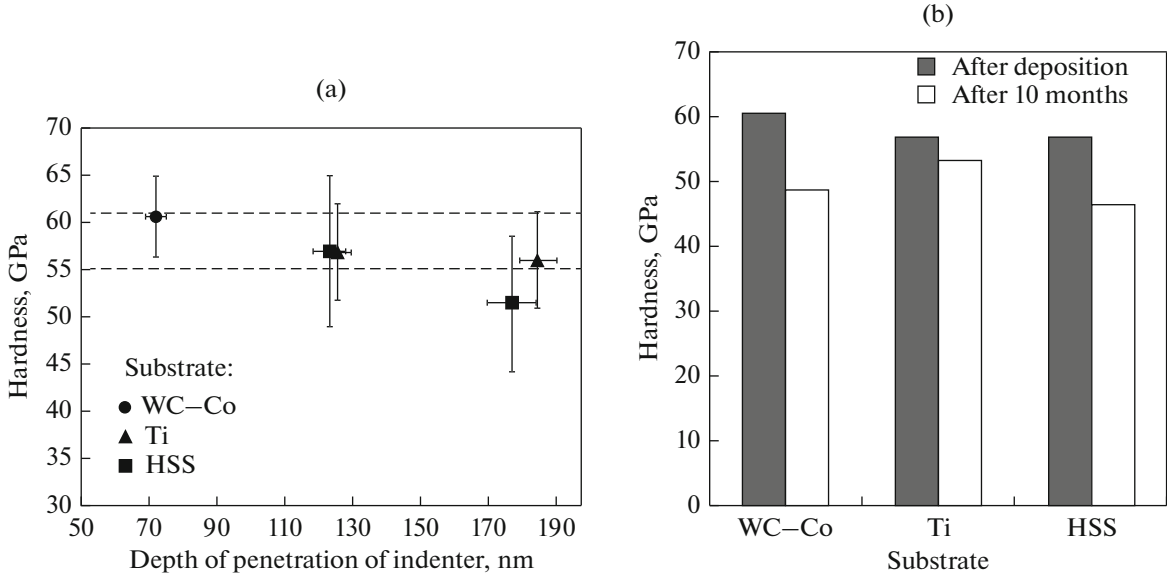

Fig. 3. Dependence of the measured values of the hardness of the TiB_2 coating (3) on (a) depth of penetration of indenter and (b) substrate material and time of testing.

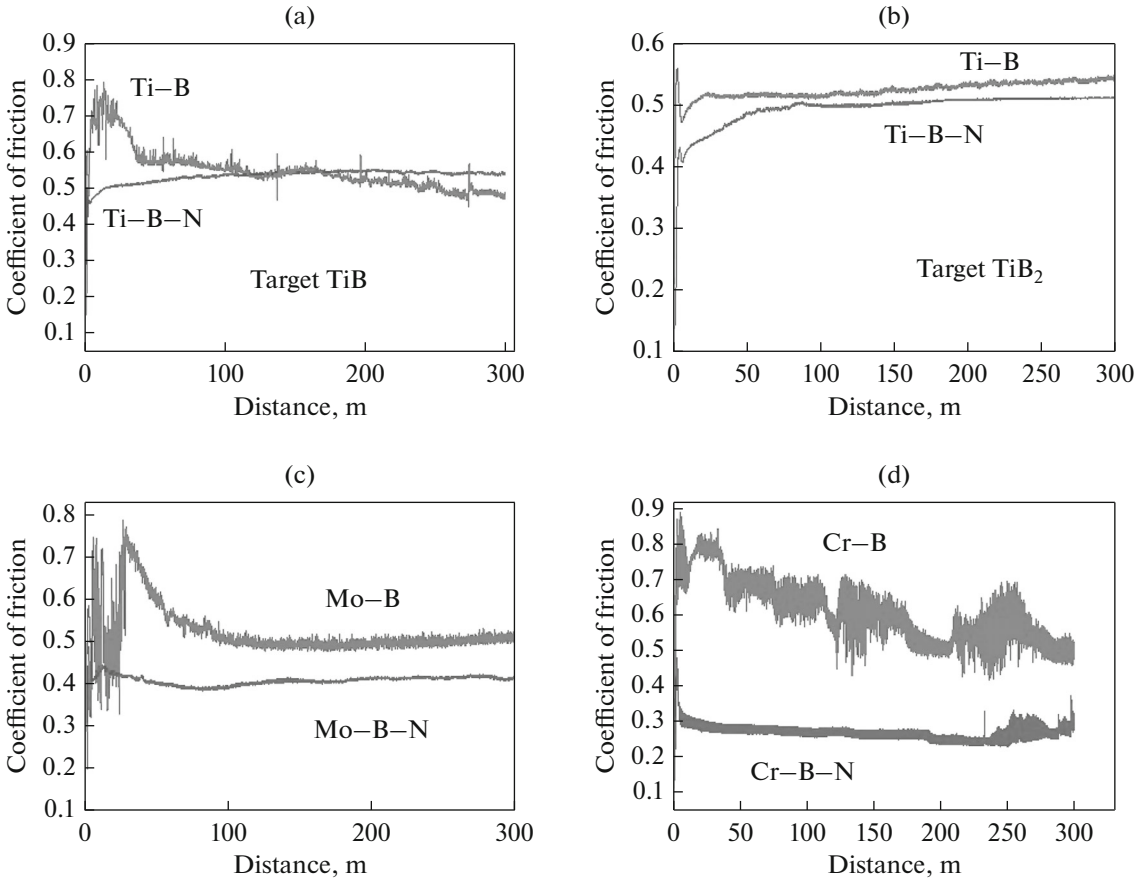

Fig. 4. Dependence of coefficient of friction on the friction path for (a) coatings 1 and 2, (b) 3 and 4, (c) 5 and 6, and (d) 7 and 8.

resistance of coatings and their behavior under conditions of localized deformation in the zone of tribological contact [26, 38, 39]. To achieve high performance characteristics, a high adhesive strength must also be ensured. The values of the critical load (L_c) that lead to the appearance of detachments upon scratch testing are presented in Table 2. The L_c values were in the range of 19–70 N. As was shown by the tests of hard-alloy tools with coatings [40], for the efficient work of a tool, the values of $L_c \geq 40$–50 N are necessary. Only coatings 5–8 meet these requirements and, therefore, they can be recommended to increase the service life of metalworking tools.

The dependences of the coefficient of friction of coatings on the distance covered by the counterbody are presented in Fig. 4. The coating 1 showed an increase in the coefficient of friction to ~0.8 on the first 40 m, after which it decreased from 0.57 to 0.47. In the case of coating 2, the stable values on the level of 0.50–0.55 during the entire cycle of testing (300 m) were observed. The similar values of the coefficient of friction were observed for coatings 3 and 4 in the Ti–B–N system. The behavior of Mo–B and Cr–B coatings was similar to coating 1 (Ti–B) as follows: after an initial maximum of 0.7–0.8, the coefficient of friction decreases to ~0.5, which is related to the full wear of the coating, as in the case of coating 1. The introduction of nitrogen led to the stabilization of the coefficient of friction and its decrease to the values of ~0.4 and ~0.3 for the Mo–B–N and Cr–B–N coatings, respectively. The values of the relative wear of coatings were determined based on the profilograms of the wear tracks obtained. The data are presented in Table 2. The minimum values of the relative wear $(0.8–1.2) \times 10^{-6}$ mm^3 N^{-1} m^{-1} were fixed for nitrogen-containing coatings. For binary boride coatings, the wear resistance was worse by an order of magnitude; the relative wear was $(16–21) \times 10^{-6}$ mm^3 N^{-1} m^{-1}. The improvement of the tribological characteristics upon introducing nitrogen in the composition of coatings can be explained by an increase of their adhesive strength (see Table 2) and crack resistance (see, e.g., [41, 42]). Also, the products of the interaction of the borides with oxygen of air with the formation of B_2O_3 and water vapor, leading to the formation of H_3BO_3, which possesses the properties of a solid grease [43], can have an influence on the tribological properties of coatings tested in a wet atmosphere.

To estimate the oxidation resistance, annealings of coatings deposited on KhN65VMTYu heat-resistant

Table 3. Resistance of coatings to high-temperature oxidation

Coating	Target	$C_{N2\%}$	Depth of oxidation (nm) at the temperature, °C					
			500	600	700	800	900	1000
1	TiB	0	390	540	800	1420		
2		15	100	400	700			
3	TiB_2	0	500	900				
4		15	300	500				
5	MoB	0	270	870				
6		15	350	1010				
7	CrB_2	0	410	660	840	940	1170	
8		15	0	0	130	300	1400	1600

* Gray fill of cells in the table corresponds to complete oxidation of coatings.

alloy were carried out. The thicknesses of the oxide layers formed on the surfaces of the coatings were calculated based on the GDOES data on the distribution of elements over the depth of the samples. The results are presented in Fig. 5 and in Table 3.

The Mo–B–(N) coatings withstood heating to 600°C. Upon a further temperature increase, the complete oxidation of the coatings accompanied by the boron burn-out (absence of B signal in the GDOES profiles) and by the formation of a loose oxide MoO_3 took place. The low oxidation resistance of the coatings in the Mo–B–(N) system is caused by the low protective properties of the arising oxide MoO_3. The oxidation resistance of the coatings deposited using

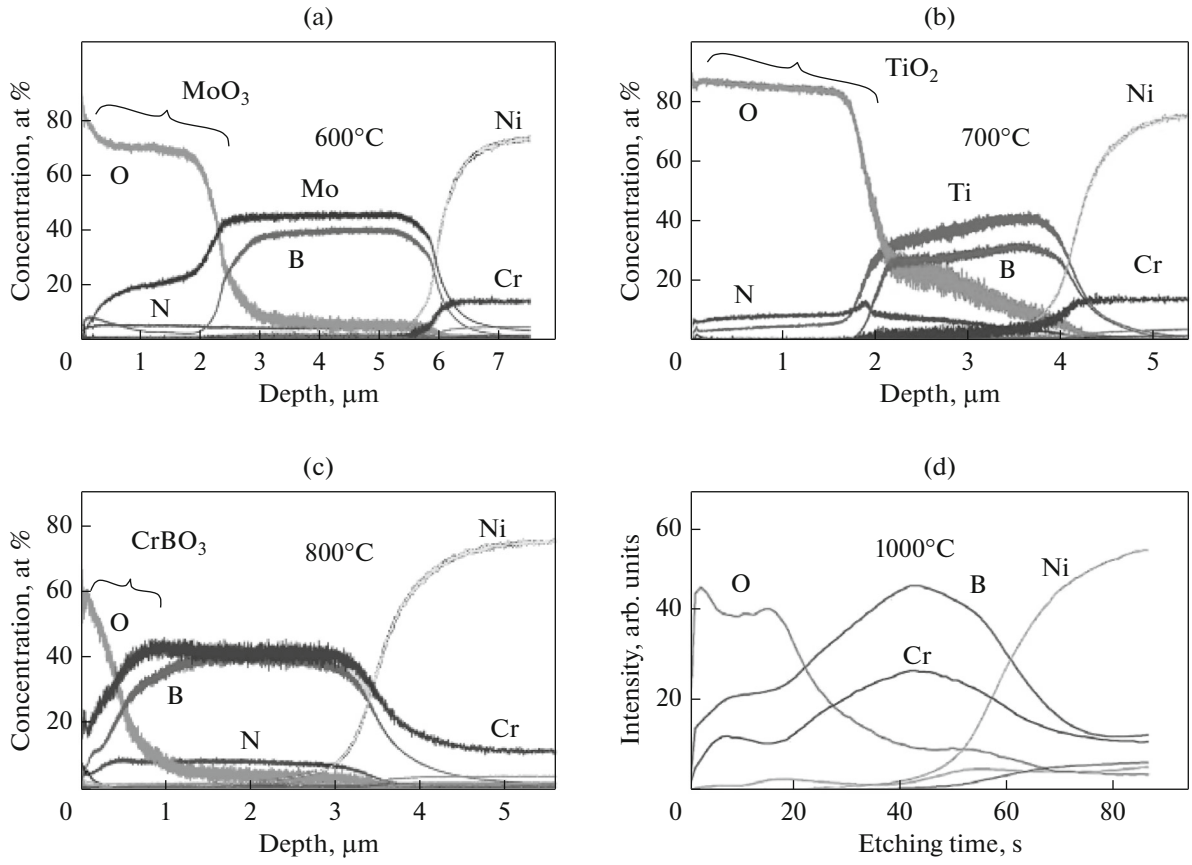

Fig. 5. Distribution of elements by depth of coating after annealings. (a) Mo–B–N no. 6, (b) Ti–B no. 1, (c, d) Cr–B–N no. 8.

the TiB_2 target was also limited to a temperature of 600°C, while the Ti–B and Ti–B–N coatings obtained using the TiB target withstood temperatures of 700 and 800°C, respectively. The lower oxidation resistance of Ti–B (coating 3) compared to other coatings in the Ti–B–N system (1, 2, 4) may be related to its texture, which facilitates the diffusion of oxygen along grain boundaries. From all of the studied samples, the highest oxidation resistance was achieved for Cr–B and Cr–B–N coatings, which can be explained by the formation of an oxide film of Cr_2O_3 and/or $CrBO_3$ [44] during heating in an air atmosphere, which prevents the further penetration of oxygen deeper into the surface. The introduction of nitrogen into the Cr–B coatings led to the suppression of the (001) texture (see Fig. 2) and a decrease in crystallite size, which finally made it possible to increase the oxidation resistance to 1000°C in comparison with 900°C for a nitrogen-free coating. The positive influence of nitrogen was observed at both low and high temperatures. For example, the oxidation of the Cr–B–N coatings was not observed up to 600°C, whereas Cr–B coatings were oxidized to depths of 410 and 660 nm, respectively, at temperatures of 500 and 600°C. The Cr–B coatings were fully oxidized at 1000°C, while in the case of Cr–B–N, the depth of oxidation did not exceed half of the coating thickness. An analysis of the GDOES profiles made it possible to find significant differences in the behavior of coatings upon oxidizing. The surface oxide layer in the case of the Ti–B–(N) and Mo–B–(N) systems contains only oxygen atoms and atoms of metals, which indicates the formation of oxide layers. For coatings 7 and 8, the oxidized layer contained chromium, oxygen, and boron atoms, which confirms the formation of the Cr_2O_3 phase, along with the $CrBO_3$-type phase described in [44].

CONCLUSIONS

Ti–B–(N), Mo–B–(N), and Cr–B–(N)C coatings were obtained by magnetron sputtering of ceramic cathodes manufactured by self-propagating high-temperature synthesis. At high values of the M/B ratio, the base of the coatings were the phases with orthorhombic (TiB) or tetragonal structure (MoB) and, at M/B ~ 0.5, predominantly phases with a hexagonal lattice (TiB_2, CrB_2) were formed. The introduction of nitrogen did not induce the formation of additional crystalline phases; however, in some cases, it led to a decrease of the size of crystallites (Ti–B–(N), TiB_2 target) and the disappearance of texture (Ti–B–(N), Cr–B–(N)).

In the Ti–B–(N) system, superhard coatings with hardnesses of $H > 40$ GPa and high elastic recovery $W = 64–72\%$ were obtained. For MoB and CrB_2 coatings, the hardness was in the range of $H = 14–39$ GPa; the value of W was 48–61%. The Ti–B–N (0.5), Mo–B–N (0.4), and Cr–B–N (0.3) coatings had the lowest values of the coefficient of friction, as well as have shown low relative wear $(0.8–1.2) \times 10^{-6}$ mm^3 N^{-1} m^{-1}.

The oxidation resistance of coatings grew in the series Mo–B–N → Mo–B → Ti–B–N → Ti–B → Cr–B → Cr–B–N. The high oxidation resistance of the Cr–B–N coatings is caused by the formation of a protective layer based on chromium compounds, i.e., Cr_2O_3 and $CrBO_3$, on their surface, which impedes the penetration of oxygen atoms into the coating.

ACKNOWLEDGMENTS

The authors are grateful to V. Mityukhlyaev for scanning electron microscopy, and M.Ya. Bychkova for tribological tests. The work was supported by the Ministry of Education and Science of the Russian Federation (state assignment no. 11.7172.2017/8.9).

REFERENCES

1. W. Wallgram and U. Schleinkofer, "Synthesis, structure, and behavior of a new CVD TiB_2 coatings with extraordinary properties for high performance applications," *Proc. 17th Plansee Seminar,* 2009, vol. 2, pp. 32/1–32/14.
2. S. Taktak, "Tribological behavior of borided bearing steels at elevated temperatures," Surf. Coat. Technol. **201**, 2230–2239 (2006).
3. H. B. Hassan and Z. A. Hamid, "Electroless Ni–B supported on carbon for direct alcohol fuel cell applications," Int. J. Hydrogen Energy **36**, 849–856 (2011).
4. L. Hejun, Y. Dongjia, F. Qiangang, L. Lei, Zh. Yulei, Y. Xiyuan, W. Yongjie, and L. Hailiang, "Anti-oxidation and ablation properties of carbon/carbon composites infiltrated by hafnium boride," Carbon **52**, 418–426 (2013).
5. R. Ribeiro, S. Ingole, M. Usta, C. Bindal, A. H. Ucisik, and H. Liang, "Tribological investigation of tantalum boride coating under dry and simulated body fluid conditions," Wear **262**, 1380–1386 (2007).
6. A. A. Goncharov, P. I. Ignatenko, V. V. Petukhov, V. A. Konovalov, G. K. Volkova, V. A. Stupak, and V. A. Glazunova, "Composition, structure and properties of tantalum boride nanostructured films," Tech. Phys. **51**, 1340–1343 (2006).
7. A. A. Goncharov, V. V. Petukhov, D. N. Terpii, P. I. Ignatenko, and V. A. Stupak, "Nanostructured films of vanadium borides," Inorg. Mater. **41**, 696–699 (2005).
8. F. Kunc, J. Musil, P. H. Mayrhofer, and C. Mitterer, "Low-stress superhard Ti–B films prepared by magnetron sputtering," Surf. Coat. Technol. **174–175**, 744–753 (2003).
9. V. Ferrando, C. Tarantini, P. Manfrinetti, I. Pallecchi, M. Salvato, and C. Ferdeghini, "Growth of diborides thin films on different substrates by pulsed laser ablation," Thin Solid Films **515**, 1439–1444 (2006).
10. B. T. Mayumi, N. Atsushi, N. Yasuo, K. Shozo, H. Masanobu, H. Yuichiro, A. Eiji, M. Hideakia, and M. Kazuya, "Low temperature deposited Zr–B film

applicable to extremely thin barrier for copper interconnect," Appl. Surf. Sci. **256**, 1222–1226 (2009).

11. A. Chatterjee, S. Jayaraman, J. E. Gerbi, N. Kumar, J. R. Abelson, P. Bellon, A. A. Polycarpou, and J. P. Chevalier, "Tribological behavior of hafnium diboride thin films," Surf. Coat. Technol. **201**, 4317–4322 (2006).
12. K. A. Khor, L. G. Yu, and G. Sundararajan, "Formation of hard tungsten boride layer by spark plasma sintering boriding," Thin Solid Films **478**, 232–237 (2005).
13. J. V. Rau, A. Latini, A. R. Generosi, V. Albertini, D. Ferro, R. Teghil, and S. M. Barinov, "Deposition and characterization of superhard biphasic ruthenium boride films," Acta Mater. **57**, 673–681 (2009).
14. Z.-W. Ji, C.-H. Hu, D.-H. Wang, Y. Zhong, J. Yang, W.-Q. Zhang, and H.-Y. Zhou, "Mechanical properties and chemical bonding of the Os–B system: A first-principles study," Acta Mater. **60**, 4208–4217 (2012).
15. F. V. Kiryukhantsev-Korneev, A. N. Sheveyko, E. A. Levashov, and D. V. Shtansky, "Perspective nanostructural coatings for machinery construction," Vopr. Materialoved., No. 2 (154), 187–201 (2008).
16. E. A. Levashov, D. V. Shtansky, Ph. V. Kiryukhantsev-Korneev, M. I. Petrzhik, M. Ya. Tyurina, and A. N. Sheveyko, "Multifunctional nanostructured coatings: Formation, structure, and the uniformity of measuring their mechanical and tribological properties," Russ. Metall. (Engl. Transl.) **2010**, 917–935 (2010).
17. H. Holzschuh, "Deposition of Ti–B–N (single and multilayer) and Zr–B–N coatings by chemical vapor deposition techniques on cutting tools," Thin Solid Films **469–470**, 92–98 (2004).
18. S. Jayaraman, J. E. Gerbi, Y. Yang, D. Y. Kim, A. Chatterjee, P. Bellon, G. S. Girolami, J. P. Chevalier, and J. R. Abelson, "HfB_2 and Hf–B–N hard coatings by chemical vapor deposition," Surf. Coat. Technol. **200**, 6629–6633 (2006).
19. A. I. Bazhin, A. A. Goncharov, V. V. Petukhov, T. D. Radjabov, V. A. Stupak, and V. A. Konovalov, "Magnetron sputtering of a vanadium-diboride target in Ar + N_2 gaseous mixtures," Vacuum **80**, 918–922 (2006).
20. P. Holubar, M. Jilek, and M. Sima, "Present and possible future applications of superhard nanocomposite coatings," Surf. Coat. Technol. **133–134**, 145–151 (2000).
21. M. Usta, I. Ozbek, C. Bindal, A. H. Ucisik, S. Ingole, and H. Liang, "A comparative study of borided pure niobium, tungsten and chromium," Vacuum **80**, 1321–1325 (2006).
22. E. N. Eremina, V. V, Kurbatkina, E. A. Levashov, A. S. Rogachev, and N. A. Kochetov, "Obtaining the composite MoB material by means of force SHS compacting with preliminary mechanical activation of Mo–10% B mixture." Chem. Sustainable Dev. **13**, 197–204 (2005).
23. V. V. Kurbatkina, E. A. Levashov, E. I. Patsera, N. A. Kochetov, and A. S. Rogachev, "Combustion and formation in the mechanoactivated Cr–B system," Int. J. Self-Propag. High-Temp. Synth. **17**, 189–194 (2008).
24. T. S. Azatyan, V. M. Mal'tsev, A. G. Merzhanov, and V. A. Seleznev, "Combustion wave propagation mechanism in titanium–boron mixtures," Combust., Explos. Shock Waves **16**, 163–167 (1980).
25. F. V. Kiryukhantsev-Korneev, "Elemental analysis of coatings by high-frequency glow discharge optical emission spectroscopy," Prot. Met. Phys. Chem. Surf. **48**, 585–590 (2012).
26. D. V. Shtansky, S. A. Kulinich, E. A. Levashov, A. N. Sheveiko, Ph. V. Kiryukhantsev-Korneev, and J. J. Moore, "Localized deformation of multicomponent thin films," Thin Solid Films **420–421**, 330–337 (2002).
27. D. V. Shtansky, K. A. Kuptsov, Ph. V. Kiryukhantsev-Korneev, and A. N. Sheveyko, "High thermal stability of TiAlSiCN coatings with "comb" like nanocomposite structure," Surf. Coat. Technol. **206**, 4840–4849 (2012).
28. S. A.Glatz, C. M. Koller, H. Bolvardi, S. Kolozsvári, H. Riedl, and P. H. Mayrhofer, "Influence of Mo on the structure and the tribomechanical properties of arc evaporated Ti–Al–N," Surf. Coat. Technol. **311**, 330–336 (2017).
29. J. M. Wheeler, R. Raghavan, V. Chawla, M. Morsteinb, and J. Michlera, "Deformation of hard coatings at elevated temperatures," Surf. Coat. Technol. **254**, 382–387 (2014).
30. D. Peak, G. W. Luther III, and D. L. Sparks, "ATR-FTIR spectroscopic studies of boric acid adsorption on hydrous ferric oxide," Geochim. Cosmochim. Acta **67**, 2551–2560 (2003).
31. A. Najafi, F. Golestani-Farda, H. R. Rezaiea, and N. Ehsania, "Effect of APC addition on precursors properties during synthesis of B_4C nano powder by a sol–gel process," J. Alloys Compd. **509**, 9164–9170 (2011).
32. D. Tsiourvas, A. Tsetsekou, M. Arkas, S. Diplas, and E. Mastrogianni, "Covalent attachment of a bioactive hyperbranched polymeric layer to titanium surface for the biomimetic growth of calcium phosphates," J. Mater. Sci.: Mater. Med. **22**, 85–96 (2011).
33. Y. Toshiya, "In-situ observation of Mo–O stretching vibrations during the reduction of Mo–O, with hydrogen by diffuse reflectance ftir spectroscopy," Appl. Surf. Sci. **40**, 179–181 (1989).
34. Z.-H. Zhou, H. Wang, P. Yu, M. M. Olmstead, and S. P. Cramer, "Structure and spectroscopy of a bidentate bis-homocitrate dioxo-molybdenum(VI) complex: Insights relevant to the structure and properties of the FeMo-cofactor in nitrogenase," J. Inorg. Biochem. **118**, 100–106 (2013).
35. T. Rainer, "Determination of the H_3BO_3 concentration in fluid and melt inclusions in granite pegmatites by laser Raman microprobe spectroscopy," Am. Mineral. **87**, 56–68 (2002).
36. Sassolite R060496. http://rruff.info/chem=H,%20B,%20O/display=default/ R060496.
37. L. Karlsson, L. Hultman, M. P. Johansson, J.-E. Sundgren, and H. Ljungcrantz, "Growth, microstructure, and mechanical properties of arc evaporated TiC_xN_{1-x}

($0 \le x \le 1$) films," Surf. Coat. Technol. **126**, 1–14 (2000).

38. A. Leyland and A. Matthews, "On the significance of the H/E ratio in wear control: A nanocomposite coating approach to optimized tribological behavior," Wear **246**, 1–11 (2000).
39. E. A. Levashov, M. I. Petrzhik, D. V. Shtansky, Ph. V. Kiryukhantsev-Korneev, A. N. Sheveiko, R. Z. Valiev, D. V. Gunderov, S. D. Prokoshkin, A. V. Korotitskiy, and A. Yu. Smolin, "Nanostructured titanium alloys and multicomponent bioactive films: Mechanical behavior at indentation," Mater. Sci. Eng., A **570**, 51–62 (2013).
40. F. V. Kiryukhatsev-Korneev, N. A. Shirmanov, A. N. Sheveyko, E. A. Levashov, M. I. Petrzhik, and D. V. Shtansky, "Nanostructural wear-resistant coatings produced on metal-cutting tools by electric- arc evaporation and magnetron sputtering," Russ. Eng. Res. **30**, 910–920 (2010).
41. C.-H. Cheng, J. W. Lee, L. W. Ho, H.-W. Chen, Y.-C. Chan, and J.-G. Duh, "Microstructure and mechanical property evaluation of pulsed DC magnetron sputtered Cr–B and Cr–B–N films," Surf. Coat. Technol. **206**, 1711–1719 (2011).
42. Ph. V. Kiryukhantsev-Korneev, J. F. Pierson, M. Y. Bychkova, O. S. Manakova, E. A. Levashov, and D. V. Shtansky, "Comparative study of sliding, scratching, and impact-loading behavior of hard CrB_2 and Cr–B–N films," Tribol. Lett. **63**, 44 (2016).
43. F. V. Kiryukhatsev-Korneev, P. A. Trukhanov, A. V. Bondarev, N. V. Shvyndina, and E. A. Levashov, "Structure and properties of tribological coatings in Cu–B system," Phys. Met. Metallogr. **115**, 716–722 (2014).
44. F. V. Kiryukhatsev-Korneev, M. I. Petrzhik, A. N. Sheveyko, E. A. Levashov, and D. V. Shtansky, "Effect of Al, Si and Cr on thermal stability and high temperature oxidation resistance of coatings based on titanium boronitride," Phys. Met. Metallogr. **104**, 167–174 (2007).

Translated by A. Bannov